Nonlinear static analysis of functionally graded porous beams under thermal effect

Şeref D. Akbaş[*]

*Department of Civil Engineering, Bursa Technical University, Yıldırım Campus,
Yıldırım, Bursa 16330, Turkey*

Abstract. This paper deals with the nonlinear static deflections of functionally graded (FG) porous under thermal effect. Material properties vary in both position-dependent and temperature-dependent. The considered nonlinear problem is solved by using Total Lagrangian finite element method within two-dimensional (2-D) continuum model in the Newton-Raphson iteration method. In numerical examples, the effects of material distribution, porosity parameters, temperature rising on the nonlinear large deflections of FG beams are presented and discussed with porosity effects. Also, the effects of the different porosity models on the FG beams are investigated in temperature rising.

Keywords: functionally graded material; porosity; nonlinear analysis; total langragian finite element model; large deflections

1. Introduction

Functionally graded materials (FGMs) are a type of composite which the properties of materials change in a direction. Generally, FGMs are used the thermal barrier systems which produced metal and ceramic materials. As compared to the conventional composite materials, FGMs perform more fracture-resistance and structural strength. With the development of technology, FGMs are used many engineering projects such as aircrafts, biomedical products, space vehicles, power plants.

During the processing in the fabrication of functionally graded materials, it can occur micro-voids and porosities in the material body due to technically problems, curing or poor-quality productions. Especially, the part of ceramic in the functionally graded materials occurs voids more frequently. It is known that the porosity is defined a measure of voids which a fraction of the volume of voids on the total volume. The porosity varies between 0 and 1. The porosity is very important issue in the mechanical behavior of structures because materials can lose their strength after a certain porosity ratio. Therefore, understanding the mechanical behavior of structural elements with porosity is importance in designs.

In the last few decades considerable interest has been focused on studying of nonlinear analysis

---

[*]Corresponding author, Ph.D., E-mail: serefda@yahoo.com

of FG beams. In the open literature, studies of the nonlinear studies of FG beams are as follows; thermal buckling load of a curved beam made of FGM with doubly symmetric cross section was investigated by Rastgo *et al.* (2005). Agarwl *et al.* (2006) analysed the large deformation behaviour of anisotropic and inhomogeneous beams using exact linear static solutions. Li *et al.* (2006) examined the thermal post-buckling of FGM clamped-clamped Timoshenko beams subjected to transversely non-uniform temperature. Based on Kirchhoff's assumption of straight normal line of beams and considering the effects of the axial elongation, the initial curvature and stretching-bending coupling on the arch deformation, geometrically nonlinear governing equations of FGM arches subjected to mechanical and thermal loads were derived by Song and Li (2008). Kang and Li (2009) studied the bending of FGM cantilever beams with power-law non-linearity subjected to an end force. Ke *et al.* (2009) investigated the post-buckling of FGM beams with an open edge crack based on the Timoshenko beam theory and von Kármán nonlinear kinematics by using the Ritz method. Kang and Li (2010) examined the large deflections of a non-linear cantilever FGM beam. The thermal post-buckling behaviour of uniform slender FGM beams was investigated independently using the classical Rayleigh-Ritz formulation and versatile finite element analysis based on the von Karman strain-displacement relations by Anandrao *et al.* (2010). Kocatürk *et al.* (2011) and Kocatürk and Akbaş (2010) investigated the full geometrically non-linear static analysis of FGM and homogeneous beams under a non-follower transversal uniformly distributed load. Fallah and Aghdam (2011) studied the nonlinear free vibration and post-buckling analysis of FGM beams on nonlinear elastic foundation. Almeida *et al.* (2011) conducted the geometric nonlinear analyses of FGM beams by using a tailored Lagrangian formulation. The thermomechanical stability of FG thin-walled cantilever pipes conveying flow and loading by compressive axial force was investigated by Hosseini and Fazelzadeh (2011). Li and Li (2011) analyzed post-buckling behavior of FG columns under distributed loads. Yan *et al.* (2012) investigated the nonlinear flexural dynamic behavior of a clamped Timoshenko beam made of FGM with an open edge crack under an axial parametric excitation, composed of a static compressive force and a harmonic excitation force based on the Timoshenko beam theory and von Kármán nonlinear kinematics. Mohanty *et al.* (2012) studied static and dynamic stability of FG ordinary and sandwich beams by using finite element method based on the Timoshenko beam theory. Kocatürk and Akbaş (2011, 2012) presented the post-buckling analysis of FGM and homogeneous Timoshenko beams under thermal loadings. Akbaş and Kocatürk (2011, 2012, 2013) presented post-buckling analysis of FGM and homogeneous beams under the influence of temperature. Kocatürk and Akbaş (2013) investigated the thermal post-buckling of FG beams considering the temperature-dependent physical properties. Akbaş (2013a) presented the ggeometrically nonlinear static analysis of edge cracked FGM Timoshenko beams subjected to a non-follower transversal point load. Nonlinear bending and thermal post-buckling of FG beams resting on an elastic foundation investigated by (Hui-Shen and Wang 2014, Li and Shao 2014, Zhang and Zhou 2014, Sun *et al.* 2016, Trinh *et al.* 2016). Babilio (2014) investigated the nonlinear dynamics of FG beams resting on a linear viscoelastic foundation under the axial time-dependent excitation. Nguyen *et al.* (2014) analyzed geometrically nonlinear of FG planar beam and frame structures by using finite element method. Akbaş (2011, 2013b, 2014 2015a, b, c, 2016a, b, 2017e) analyzed post-buckling, dynamics of cracked and axially graded FG beams. Elmaguiri *et al.* (2015) studied the large-amplitude free vibration of clamped immovable thin FG beams. Kolakowski and Teter (2015) studied static coupled buckling of thin-walled FG columns with trapezoidal and square cross-sections. Amara *et al.* (2016) investigated post-buckling of simply supported FG beams using various shear deformation theories. Akbarzadeh Khorshidi *et al.*
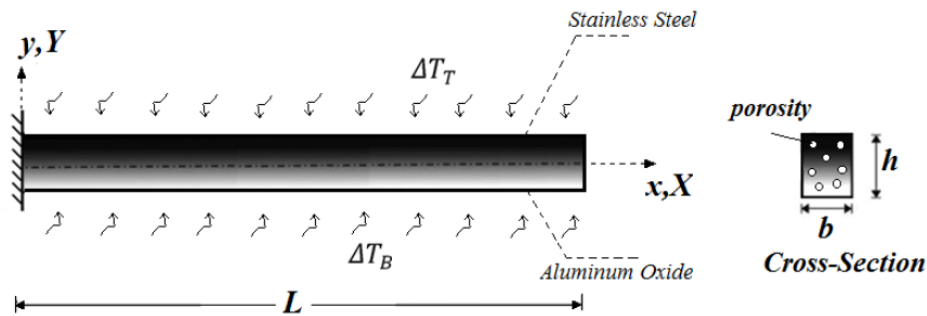
Fig. 1 A cantilever FG beam with porosity subjected to non-uniform temperature rising

(2016) analysed post-buckling of shear deformable FG nanobeams based on modified couple stress theory with von-Karman geometric nonlinearity. Kar and Panda (2016) examined the nonlinear free vibration of FG panels under nonlinear temperature field.

In the literature, studies of the porosity effect in the FG structures are as follows; Wattanasakulpong and Ungbhakorn (2014) studied linear and nonlinear vibration FG beams with porosity effects. Mechab *et al.* (2016a, 2016b) examined free vibration analysis of a FG nano-plate resting on elastic foundations with the porosities effect. Şimşek and Aydın (2017) examined forced vibration of FG microplates with porosity effects based on the modified couple stress theory. Jahwari and Naguib (2016) investigated FG viscoelastic porous plates with a higher order plate theory and statistical based model of cellular distribution. Akbaş (2017a, b, c, d) examined vibration, buckling and post-buckling of FG porous structures. Vibration characteristics of FG beams with porosity effect and various thermal loadings are investigated by (Ebrahimi and Jafari 2016, Ebrahimi *et al.* 2016).

It is seen from literature study that nonlinear analysis of FG porous beams with thermal effects has not been investigated so far. The primary purpose of this study is to fill this gap for FG beams. The considered problem is solved by using the total Lagrangian finite element model of two-dimensional (2-D) continuum by taking into account full geometric nonlinearity. The effects of material distribution, temperature rising and porosity parameters on the large deflections of FG beams are investigated with different porosity models in the temperature-dependent physically properties. Also, the difference among the porosity models is investigated in detail.

2. Theory and formulation

A FG cantilever beam of length L, width b, and height h, subjected to non-uniform temperature rising along the thickness direction as shown in Fig. 1 with material or Lagrangian coordinate system (X,Y,Z) and with spatial or Euler coordinate system (x,y,z). The FG beam is made porous materials and vary though height direction. Temperature rising of the bottom surface indicates as ΔT_B, whereas temperature rising of the top surface indicates as ΔT_T.

The material properties of the beam are both position-dependent and temperature-dependent. The effective material properties of the FG beam, P, i.e., Elasticity modulus E, coefficient of thermal expansion α_X, coefficient of thermal conductivity k, Poisson's ratio v, and shear modulus G vary continuously in the thickness direction (Y axis) according to a power-law function and a function of temperature T (see Touloukian 1967) as follows

Table 1 The coefficients of temperature *T* for Aluminum Oxide (from Reddy and Chin 1998)

The material properties	P_0	P_{-1}	P_1	P_2	P_3
Thermal expansion coefficient α_X (1/K)	6.8269×10^{-6}	0	1.838×10^{-4}	0	0
Young's modulus E (Pa)	349.55×10^9	0	-3.853×10^{-4}	4.027×10^{-7}	-1.673×10^{-10}
Poisson's ratio v	0.2600	0	0	0	0
Coefficient of thermal conductivity k (W/mK)	-14.087	-1123.6	-6.227×10^{-3}	0	0

Table 2 The coefficients of temperature *T* for Stainless Steel (from Reddy and Chin 1998)

The material properties	P_0	P_{-1}	P_1	P_2	P_3
Thermal expansion coefficient α_X (1/K)	12.330×10^{-6}	0	8.086×10^{-4}	0	0
Young's modulus E (Pa)	201.04×10^9	0	3.079×10^{-4}	-6.534×10^{-7}	0
Poisson's ratio v	0.3262	0	-2.002×10^{-4}	3.797×10^{-7}	0
Coefficient of thermal conductivity k (W/mK)	15.379	0	-1.264×10^{-3}	2.092×10^{-6}	-7.223×10^{-10}

$$P(Y,T) = (P_T(T) - P_B(T))\left(\frac{Y}{h} + \frac{1}{2}\right)^n + P_B(T) \tag{1a}$$

$$P(T) = P_0(P_{-1}T^{-1} + 1 + P_1T + P_2T^2 + P_3T^3) \tag{1b}$$

where P_T and P_B are the material properties of the top and the bottom surfaces of the beam that depends on temperature (T). $T=T_0+\Delta T$, where T_0 is installation temperature and ΔT is the temperature rise. n is the non-negative power-law exponent (material distribution parameter) which dictates the material variation profile through the thickness of the beam. It is clear from Eq. (1) that when $Y=-h/2$, $P=P_B$, and when $Y=h/2$, $P=P_T$. When $n=0$ (full top material) or $n=\infty$ (full bottom material), the material of the beam is homogeneous according to Eq. (1a). In Eq. (1b), P_{-1}, P_0, P_1, P_2 and P_3 indicate the coefficients of temperature T and are unique to the constituent materials. In this study, the unit of the temperature is Kelvin (K), the unit of the Young's modulus E is Pascal (Pa) and the unit of the thermal expansion coefficient α_X is $1/K$. The beams considered in numerical examples are made of Aluminum Oxide and Stainless Steel. The bottom surface of the FG beam is Aluminum Oxide and the top surface of the FG beam is Stainless Steel. The coefficients of temperature T for Aluminum Oxide and Stainless Steel are listed in Tables 1 and 2 (from Reddy and Chin 1998).

The temperature rise $\Delta T=\Delta T(Y)$ is governed by heat transfer equation of

$$-\frac{d}{dY}\left[k(Y)\frac{d\Delta T(Y)}{dY}\right] = 0 \tag{2}$$
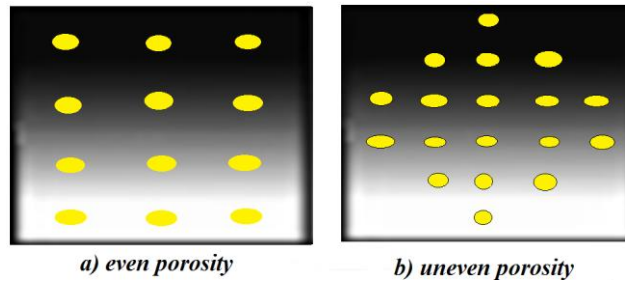
a) even porosity   *b) uneven porosity*

Fig. 2 Porosity models for FG material

By integrating Eq. (2) using boundary conditions $\Delta T(h/2)=\Delta T_T$ and $\Delta T(-h/2)=\Delta T_B$, the following expression can be obtained

$$\Delta T(Y) = \Delta T_B + \left(\Delta T_T - \Delta T_B\right) \int_{-h/2}^{y} \frac{1}{k(Y)} dY \bigg/ \int_{-h/2}^{h/2} \frac{1}{k(Y)} dY \qquad (3)$$

where k is the coefficient of thermal conductivity and dependence on Y coordinate are given by Eq. (1).

In the porosity effect for imperfect FG beam, two porosities models (even and uneven) are used which were given by Wattanasakulpong and Ungbhakorn (2014) for the power law distribution. In the even porosity model, the porosity spread uniformly though height direction. In the uneven porosity model, the porosity spread functionally though height direction. The distributions of the even and uneven porosity distributions are shown in Fig. 2.

According to the power law distribution, the effective material property for the even porosity can be expressed as follows

$$P(Y,T) = \left(P_T - P_B\right)\left(\frac{Y}{h} + \frac{1}{2}\right)^n + P_B - \left(P_T + P_B\right)\frac{a}{2} \qquad (4)$$

where a ($a \ll 1$) is the volume fraction of porosities. When $a=0$, the beam becomes perfect FGM. For uneven porosity distribution, the effective material property can be expressed as follows according to the power law distribution

$$P(Y,T) = \left(P_T - P_B\right)\left(\frac{Y}{h} + \frac{1}{2}\right)^n + P_B - \left(P_T + P_B\right)\frac{a}{2}\left(1 - \frac{2\,|\,Y|}{h}\right) \qquad (5)$$

In the comparison of the two models: In uneven porosity model, the voids stack in the middle of the beam or the neutral of the beam. So, the stiffness of the cross-section is less effected from negative influences of the porosity because the neutral axis and its adjacent areas have low stress. However, the voids stack uniformly in the whole area of the beam in the even porosity model. Hence, the stiffness of the cross-section seriously decreases seriously in the even model. As result, the rigidity of the beam in even porosity model is lower than the rigidity of the beam in uneven porosity model.

It is known that the large deflection is a geometrically nonlinear problem. In the nonlinear kinematic model of the beam for the large deflection problem, total Lagrangian approximation is used within the 2-D solid continuum model. In the solution of the nonlinear problem, finite element method is used for total Lagrangian kinematic model for an eight-node quadratic element.

The total Lagrangian finite element formulations of the problem are developed for porosity FGM beam by using the formulations given by Reddy (2014) and for isotropic and homogeneous beam material.

In the solution of the nonlinear finite element of total Lagrangian formulations, small-step incremental approaches from known solutions are used. As it is known, it is possible to obtain solutions in a single increment of the external force only in the case of mild nonlinearity (and no path dependence). To obtain realistic answers, physical insight into the nature of the problem and, usually, small-step incremental approaches from known solutions are essential. Such increments are always required if the constitutive law relating stress and strain changes is path dependent. Also, such incremental procedures are useful to reduce excessive numbers of iterations and in following the physically correct path. In the iterations, the temperature rising is divided by a suitable number according to the value of temperature. The temperature rising is divided by large numbers. After completing an iteration process, the temperature is increased by adding temperature increment to the accumulated temperature.

In this study, small-step incremental approaches from known solutions with Newton-Raphson iteration method are used in which the solution for $n+1$th load increment and i th iteration is obtained in the following form

$$d\mathbf{u}_n^i = (\mathbf{K}_T^i)^{-1}\mathbf{R}_{n+1}^i \tag{6}$$

where $\mathbf{K}_T^i$ is the tangent stiffness matrix corresponding to a tangent direction at the i th iteration, $d\mathbf{u}_n^i$ is the solution increment vector at the i th iteration and $n+1$th load increment, $\mathbf{R}_{n+1}^i$ is the residual vector at the i th iteration and $n+1$th load increment. This iteration procedure is continued until the difference between two successive solution vectors is less than a selected tolerance criterion in Euclidean norm given by

$$\sqrt{\frac{\left[(d\mathbf{u}_n^{i+1} - d\mathbf{u}_n^i)^T(d\mathbf{u}_n^{i+1} - d\mathbf{u}_n^i)\right]^2}{\left[(d\mathbf{u}_n^{i+1})^T(d\mathbf{u}_n^{i+1})\right]^2}} \le \zeta_{tol} \tag{7}$$

A series of successive approximations gives

$$\mathbf{u}_{n+1}^{i+1} = \mathbf{u}_{n+1}^i + d\mathbf{u}_{n+1}^i = \mathbf{u}_n + D\mathbf{u}_n^i \tag{8}$$

Where

$$D\mathbf{u}_n^i = \mathop{a}\limits_{k=1}^{i} \; d\mathbf{u}_n^k \tag{9}$$

The tangent stiffness matrix $\mathbf{K}_T^i$ and the residual vector $\mathbf{R}_{n+1}^i$ which are to be used in Eq. (6) at the i th iteration for the total Lagrangian finite element model of two dimensional continua for an eight-node quadratic element are given below

$$\begin{bmatrix} \mathbf{K}^{11L} + \mathbf{K}^{11NL} & \mathbf{K}^{12L} \\ \mathbf{K}^{21L} & \mathbf{K}^{22L} + \mathbf{K}^{22NL} \end{bmatrix}^i \left\{ \begin{array}{c} \overline{\mathbf{u}} \\ \overline{\mathbf{v}} \end{array} \right\}^i = \left\{ \begin{array}{c} {}_0^2\mathbf{F}^1 - {}_0^1\mathbf{F}^1 \\ {}_0^2\mathbf{F}^2 - {}_0^1\mathbf{F}^2 \end{array} \right\}^i \tag{10}$$

where

$$K_{ij}^{11L} = b\int_{\Omega^e}\left[{}_0C_{11}\left(1+\frac{\partial u}{\partial X}\right)^2\frac{\partial\psi_i}{\partial X}\frac{\partial\psi_j}{\partial X} + {}_0C_{22}\left(\frac{\partial u}{\partial Y}\right)^2\frac{\partial\psi_i}{\partial Y}\frac{\partial\psi_j}{\partial Y}\right.$$
$$+{}_0C_{12}\left(1+\frac{\partial u}{\partial X}\right)\frac{\partial u}{\partial Y}\left(\frac{\partial\psi_i}{\partial X}\frac{\partial\psi_j}{\partial X}+\frac{\partial\psi_i}{\partial Y}\frac{\partial\psi_j}{\partial X}\right)$$
$$\left.+{}_0C_{66}\left[\left(1+\frac{\partial u}{\partial X}\right)\frac{\partial\psi_i}{\partial Y}+\frac{\partial u}{\partial Y}\frac{\partial\psi_i}{\partial X}\right]\times\left[\left(1+\frac{\partial u}{\partial X}\right)\frac{\partial\psi_j}{\partial Y}+\frac{\partial u}{\partial Y}\frac{\partial\psi_j}{\partial X}\right]\right]dXdY \tag{11a}$$

$$K_{ij}^{12L} = b\int_{\Omega^e}\left[{}_0C_{11}\left(1+\frac{\partial u}{\partial X}\right)\frac{\partial v}{\partial X}\frac{\partial\psi_i}{\partial X}\frac{\partial\psi_j}{\partial X} + {}_0C_{22}\left(1+\frac{\partial v}{\partial Y}\right)\frac{\partial u}{\partial Y}\frac{\partial\psi_i}{\partial Y}\frac{\partial\psi_j}{\partial Y}\right.$$
$$+{}_0C_{12}\left(1+\frac{\partial u}{\partial X}\right)\left[\left(1+\frac{\partial v}{\partial Y}\right)\frac{\partial\psi_i}{\partial X}\frac{\partial\psi_j}{\partial Y}+\frac{\partial u}{\partial Y}\frac{\partial v}{\partial X}\frac{\partial\psi_i}{\partial Y}\frac{\partial\psi_j}{\partial X}\right]$$
$$\left.+{}_0C_{66}\left[\left(1+\frac{\partial u}{\partial X}\right)\frac{\partial\psi_i}{\partial Y}+\frac{\partial u}{\partial Y}\frac{\partial\psi_i}{\partial X}\right]\times\left[\left(1+\frac{\partial v}{\partial Y}\right)\frac{\partial\psi_j}{\partial X}+\frac{\partial v}{\partial X}\frac{\partial\psi_j}{\partial Y}\right]\right]dXdY = K_{ij}^{21L} \tag{11b}$$

$$K_{ij}^{22L} = b\int_{\Omega^e}\left[{}_0C_{11}\left(\frac{\partial v}{\partial X}\right)^2\frac{\partial\psi_i}{\partial X}\frac{\partial\psi_j}{\partial X} + {}_0C_{22}\left(1+\frac{\partial v}{\partial Y}\right)^2\frac{\partial\psi_i}{\partial Y}\frac{\partial\psi_j}{\partial Y}\right.$$
$$+{}_0C_{12}\left(1+\frac{\partial v}{\partial Y}\right)\frac{\partial v}{\partial X}\left(\frac{\partial\psi_i}{\partial X}\frac{\partial\psi_j}{\partial Y}+\frac{\partial\psi_i}{\partial Y}\frac{\partial\psi_j}{\partial X}\right)$$
$$\left.+{}_0C_{66}\left[\left(1+\frac{\partial v}{\partial Y}\right)\frac{\partial\psi_i}{\partial X}+\frac{\partial v}{\partial X}\frac{\partial\psi_i}{\partial Y}\right]\times\left[\left(1+\frac{\partial v}{\partial Y}\right)\frac{\partial\psi_j}{\partial X}+\frac{\partial v}{\partial X}\frac{\partial\psi_j}{\partial Y}\right]\right]dXdY \tag{11c}$$

$$K_{ij}^{11NL} = h_e\int_{\Omega^e}\left[{}_0^1S_{11}\frac{\partial\psi_i}{\partial X}\frac{\partial\psi_j}{\partial X} + {}_0^1S_{12}\left(\frac{\partial\psi_i}{\partial Y}\frac{\partial\psi_j}{\partial X}+\frac{\partial\psi_i}{\partial X}\frac{\partial\psi_j}{\partial Y}\right)\right.$$
$$\left.+{}_0^1S_{22}\frac{\partial\psi_i}{\partial Y}\frac{\partial\psi_j}{\partial Y}\right]dXdY = K_{ij}^{22N} \tag{11d}$$

$${}_0^2F_i^1 = b\int_{\Omega^e}{}_0^2f_x\,\psi_i\,dXdY + b\int_{\Gamma^e}{}_0^2t_x\,\psi_i\,ds \tag{11e}$$

$${}_0^2F_i^2 = b\int_{\Omega^e}{}_0^2f_y\,\psi_i\,dXdY + b\int_{\Gamma^e}{}_0^2t_y\,\psi_i\,ds \tag{11f}$$

where ${}_0^2f_x$, ${}_0^2f_y$ are the body forces, ${}_0^2t_x$, ${}_0^2t_y$ are the surface forces in the x and y directions. u and v are displacements in the x and y directions, ψ indicates the shape functions.

$${}_0^1F_i^1 = b\int_{\Omega^e}\left[\left(1+\frac{\partial u}{\partial X}\right)\frac{\partial\psi_i}{\partial X}{}_0^1S_{11} + \frac{\partial u}{\partial Y}\frac{\partial\psi_i}{\partial Y}{}_0^1S_{22}\right.$$
$$\left.+\left[\left(1+\frac{\partial u}{\partial X}\right)\frac{\partial\psi_i}{\partial Y}+\frac{\partial u}{\partial Y}\frac{\partial\psi_i}{\partial X}\right]{}_0^1S_{12}\right]dXdY \tag{12a}$$

$$
{}^1_0F^2_i = b \int_{\Omega^e} \left[\frac{\partial v}{\partial X} \frac{\partial \psi_i}{\partial X} {}^1_0S_{11} \right.
$$

$$
+ \left(1 + \frac{\partial v}{\partial Y} \right) \frac{\partial \psi_i}{\partial Y} {}^1_0S_{22}
$$

$$
\left. + \left[\left(1 + \frac{\partial v}{\partial Y} \right) \frac{\partial \psi_i}{\partial X} + \frac{\partial v}{\partial X} \frac{\partial \psi_i}{\partial Y} \right] {}^1_0S_{12} \right] dXdY
$$

(12b)

The constitutive relation between the second Piola-Kirchhoff stress tensor and the Green-Lagrange strain tensor can be expressed as follows

$$
{}^1_0S = \begin{Bmatrix} {}^1_0S_{11} \\ {}^1_0S_{22} \\ {}^1_0S_{12} \end{Bmatrix} = \begin{bmatrix} {}_0C_{11} & {}_0C_{12} & 0 \\ {}_0C_{12} & {}_0C_{22} & 0 \\ 0 & 0 & {}_0C_{66} \end{bmatrix} \begin{Bmatrix} {}^1_0E_{11} - \alpha_x(Y,T)\,\Delta T(T) \\ {}^1_0E_{22} \\ 2\,{}^1_0E_{12} \end{Bmatrix}
$$

(13)

where ${}^1_0S_{11}$, ${}^1_0S_{22}$, ${}^1_0S_{12}$ are the components of the second Piola-Kirchhoff stress tensor components in the initial configuration of the body, ${}^1_0E_{ij}$ are the components of the Green-Lagrange strain tensor, ${}_0C_{ij}$ are the components of the reduced constitutive tensor in the initial configuration of the body. The components of the reduced constitutive tensor can be written in terms of Young modulus E and Poisson's ratio v and their dependence on Y coordinate and temperature T are given by Eqs. (1), (4) and (5) for porosity effect, as follows

$$
{}_0C_{11} = \frac{E(Y,T)}{1 - v^2(Y,T)} \ , \ {}_0C_{12} = {}_0C_{21} = \frac{v(Y,T)\,E(Y,T)}{1 - v^2(Y)} \ ,
$$

(14)

$$
{}_0C_{22} = \frac{E(Y,T)}{1 - v^2(Y,T)} \ , \ {}_0C_{66} = \frac{E(Y,T)}{2(1 + v(Y,T))}
$$

The Green-Lagrange strain tensor is expressed in terms of displacements in the case of two-dimensional solid continuum as follows

$$
{}^1_0E = \begin{Bmatrix} {}^1_0E_{11} \\ {}^1_0E_{22} \\ 2\,{}^1_0E_{12} \end{Bmatrix} = \begin{Bmatrix} \dfrac{\partial u}{\partial X} + \dfrac{1}{2}\left[\left(\dfrac{\partial u}{\partial X}\right)^2 + \left(\dfrac{\partial v}{\partial X}\right)^2 \right] \\ \dfrac{\partial v}{\partial Y} + \dfrac{1}{2}\left[\left(\dfrac{\partial u}{\partial Y}\right)^2 + \left(\dfrac{\partial v}{\partial Y}\right)^2 \right] \\ \dfrac{\partial u}{\partial Y} + \dfrac{\partial v}{\partial X} + \left(\dfrac{\partial u}{\partial X}\dfrac{\partial u}{\partial Y} + \dfrac{\partial v}{\partial X}\dfrac{\partial v}{\partial Y} \right) \end{Bmatrix}
$$

(15)

In the finite element model, eight-node plane element is used as shown in Fig. 3.
These total displacement fields and incremental displacement fields are interpolated as follows

$$
u = \begin{Bmatrix} u \\ v \end{Bmatrix} = \begin{Bmatrix} \sum_{j=1}^{8} u_j \psi_j(x) \\ \sum_{j=1}^{8} v_j \psi_j(x) \end{Bmatrix} = [\Psi]\{\Delta\}
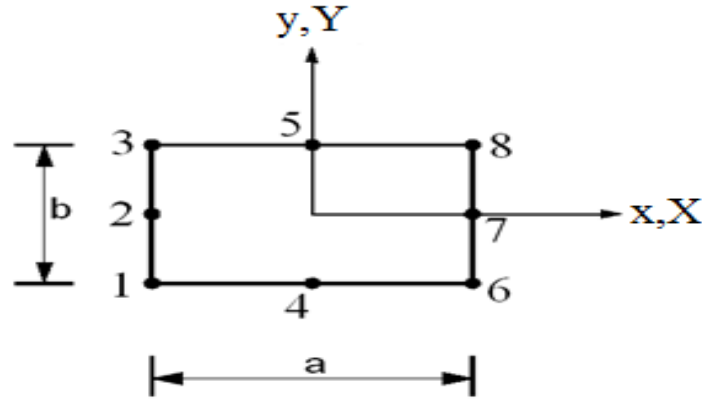$$

(16)

Fig. 3 Eight-node plane element

$$\bar{u} = \begin{bmatrix} \bar{u} \\ \bar{v} \end{bmatrix} = \begin{bmatrix} \sum_{j=1}^{8} \bar{u}_j \psi_j(x) \\ \sum_{j=1}^{8} \bar{v}_j \psi_j(x) \end{bmatrix} = [\Psi]\{du\} \tag{17}$$

where

$$[\psi] = \begin{bmatrix} \psi_1 & 0 & \psi_2 & 0 & \psi_3 & 0 & \psi_4 & 0 & \psi_5 & 0 & \psi_6 & 0 & \psi_7 & 0 & \psi_8 & 0 \\ 0 & \psi_1 & 0 & \psi_2 & 0 & \psi_3 & 0 & \psi_4 & 0 & \psi_5 & 0 & \psi_6 & 0 & \psi_7 & 0 & \psi_8 \end{bmatrix} \tag{18}$$

$$\{D\}^T = \{u_1 \ v_1 \ u_2 \ v_2 \ u_3 \ v_3 \ u_4 \ v_4 \ u_5 \ v_5 \ u_6 \ v_6 \ u_7 \ v_7 \ u_8 \ v_8\} \tag{19}$$

$$\{du\}^T = \{\bar{u}_1 \ \bar{v}_1 \ \bar{u}_2 \ \bar{v}_2 \ \bar{u}_3 \ \bar{v}_3 \ \bar{u}_4 \ \bar{v}_4 \ \bar{u}_5 \ \bar{v}_5 \ \bar{u}_6 \ \bar{v}_6 \ \bar{u}_7 \ \bar{v}_7 \ \bar{u}_8 \ \bar{v}_8\} \tag{20}$$

Shape functions for an eight-node element are as follows

$$
\begin{aligned}
[\psi_1] &= \left(X - \frac{a}{2}\right)\left(Y - \frac{b}{2}\right)\left(\frac{1}{ab} - \frac{2X_1}{a^2 b} - \frac{2Y}{ab^2}\right) \\
[\psi_2] &= \left(\frac{4}{b^2 a}\right)\left(X - \frac{a}{2}\right)\left(Y + \frac{b}{2}\right)\left(Y - \frac{b}{2}\right) \\
[\psi_3] &= \left(X - \frac{a}{2}\right)\left(Y + \frac{b}{2}\right)\left(\frac{1}{ab} + \frac{2X}{a^2 b} - \frac{2Y}{ab^2}\right) \\
[\psi_4] &= \left(\frac{4}{ba^2}\right)\left(X - \frac{a}{2}\right)\left(X + \frac{a}{2}\right)\left(Y - \frac{b}{2}\right) \\
[\psi_5] &= \left(\frac{4}{ba^2}\right)\left(X - \frac{a}{2}\right)\left(X + \frac{a}{2}\right)\left(Y + \frac{b}{2}\right) \\
[\psi_6] &= \left(X + \frac{a}{2}\right)\left(Y - \frac{b}{2}\right)\left(\frac{1}{ab} - \frac{2X}{a^2 b} + \frac{2Y}{ab^2}\right) \\
[\psi_7] &= \left(-\frac{4}{b^2 a}\right)\left(X + \frac{a}{2}\right)\left(Y - \frac{b}{2}\right)\left(Y + \frac{b}{2}\right) \\
[\psi_8] &= \left(X + \frac{a}{2}\right)\left(Y + \frac{b}{2}\right)\left(-\frac{1}{ab} + \frac{2X}{a^2 b} + \frac{2Y}{ab^2}\right)
\end{aligned}
\tag{21}
$$

Numerical calculations of the integrals seen in the rigidity matrices will be performed by using five-point Gauss rule.

3. Numerical results

In the numerical examples, large deflections, namely geometrically nonlinear deflections of the cantilever FG beam are calculated and presented for different power-law exponents, temperature rising values and porosity coefficients under non-uniform temperature rising (Fig. 1) in the temperature-dependent physically properties. The difference between of the porosity models is investigated in the large deflections. Using the conventional assembly procedure for the finite elements, the tangent stiffness matrix and the residual vector are obtained from the element stiffness matrices and residual vectors in the total Lagrangian sense for finite element model of 2-D solid continuum. After that, the solution process outlined in the preceding section is used to obtain the solution for the problem of concern. In obtaining the numerical results, graphs and solution of the nonlinear finite element model, MATLAB program is used.

It is mentioned before that the FG porous beam considered in numerical examples is made of Aluminum Oxide (bottom surface) and Stainless Steel (top surface). In numerical examples, the initial temperature (installation temperature) of the beam is assumed to be T_0=300 K. The dimensions of the beam are considered as follows: b=0.3 m, h=0.3 m, L=4 m in the numerical examples.

In order to obtain the optimum number of the finite element for the numerical calculations, the convergence study is performed in Fig. 4. In Fig. 4, maximum vertical displacements (at the free end of the beam), Cauchy normal stress at the fixed end on the top fiber of the beam and normal strain at the fixed end on the top fiber of the beam are calculated for different numbers of finite elements, the power-law exponent n=0.1, the porosity parameter a=0.2 for even porosity model for the non-uniform temperature rising in the values of ΔT_B=800 K and ΔT_T=0 K in the temperature-dependent physically property. It is noted that the finite element of the FG beam is chosen to be equal in X and Y directions in order to obtain sensitive results. In Fig. 4, m_X and m_Y indicate the number of finite element in X and Y directions, respectively.

Fig. 4 shows that the post-buckling maximum displacements, Cauchy stress and normal strian converge perfectly after the finite element m_X=m_Y=25. So, the number of finite elements is taken as 25 in both X and Y directions in the numerical calculations.

In Figs. 5 and 6, the effect of the porosity parameter (a) and porosity models on the maximum thermal nonlinear deflections (v_{max}) of the FG beam are presented in the temperature-dependent physically property and the temperature-independent physically property, respectively for n=0.3 with the non-uniform temperature rising. It is noted that, non-uniform temperature rising is considered as the temperature rising of the bottom surface ΔT_B is changed, whereas the temperature of the top surface ΔT_T is not changed ($\Delta T_T = 0$) in the numerical calculations. So, the temperature only rises at the bottom surface of the FG beam.

It is seen from Fig. 5 that the results of the even porosity model are bigger than uneven model's in the high values of temperatures for the temperature-dependent physically property. However, the results of the uneven porosity model are bigger than even model's in small and medium values of temperatures for the temperature-dependent physically property. In the results of the temperature-independent physically property, the uneven porosity model is bigger than even model's in all temperature values as seen from Fig. 6. It shows that large thermal deflection responses of FG beams significantly change in the temperature-dependent or independent physically properties. Also, it is seen from Figs. 5(a) and 6(a) that the results in between the even porosity model and uneven porosity model coincide with each other in case of a=0 (perfect FG beam) because the porosity effect is not considered. In addition, the increase in temperature causes
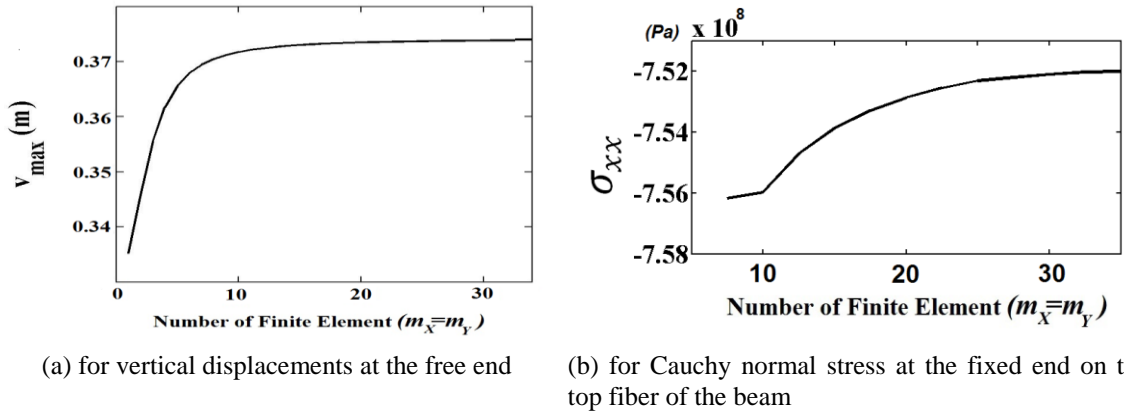
(a) for vertical displacements at the free end

(b) for Cauchy normal stress at the fixed end on the top fiber of the beam

Fig. 4 Convergence study

(a) for $a=0$ (Perfect FG beam)
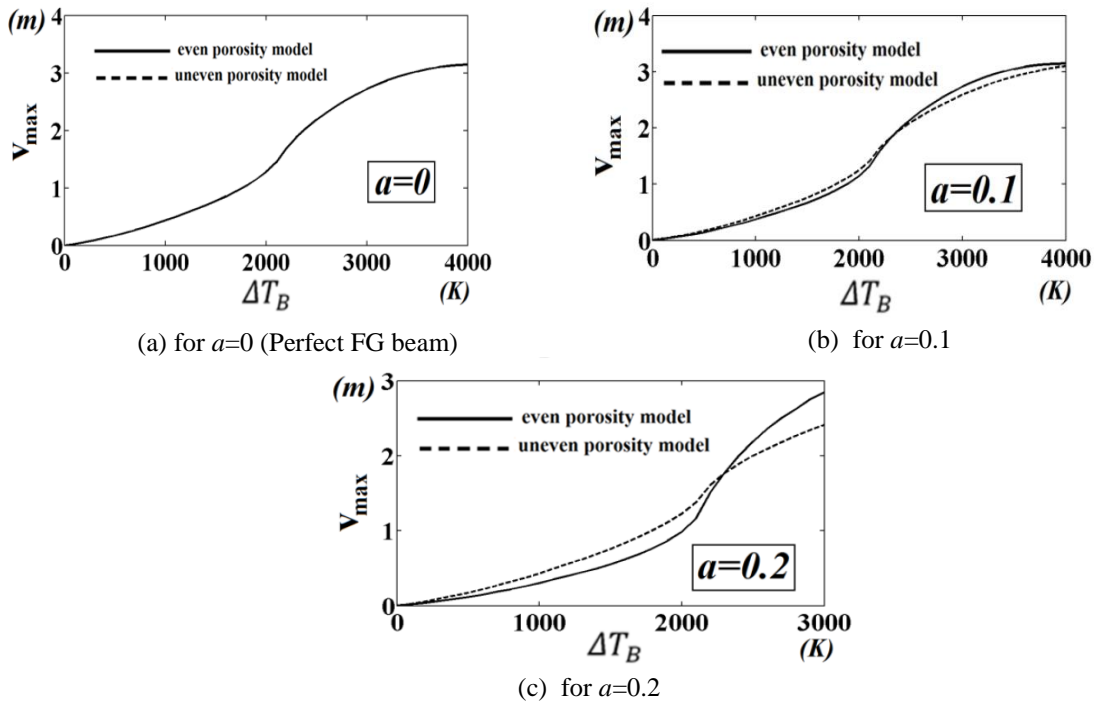
(b) for $a=0.1$

(c) for $a=0.2$

Fig. 5 Temperature rising-maximum vertical displacements (v_{max}) curves for different the porosity parameter in the temperature-dependent physically property

increase in difference of the porosity models as seen from figures. In small temperature values, difference among the porosity models is quite small. In small temperature values, the porosity is less effective in the mechanical behaviour of the FG beam.

Fig. 7 shows that the relationship between of porosity parameter a and the maximum displacements of the FG porous beam in both the temperature-dependent physically property and the temperature-independent physically property for different porosity models for $n=2$ for $\Delta T_B = 3000\,K$ and $\Delta T_T = 0$.

(a) for $a=0$ (Perfect FG beam)
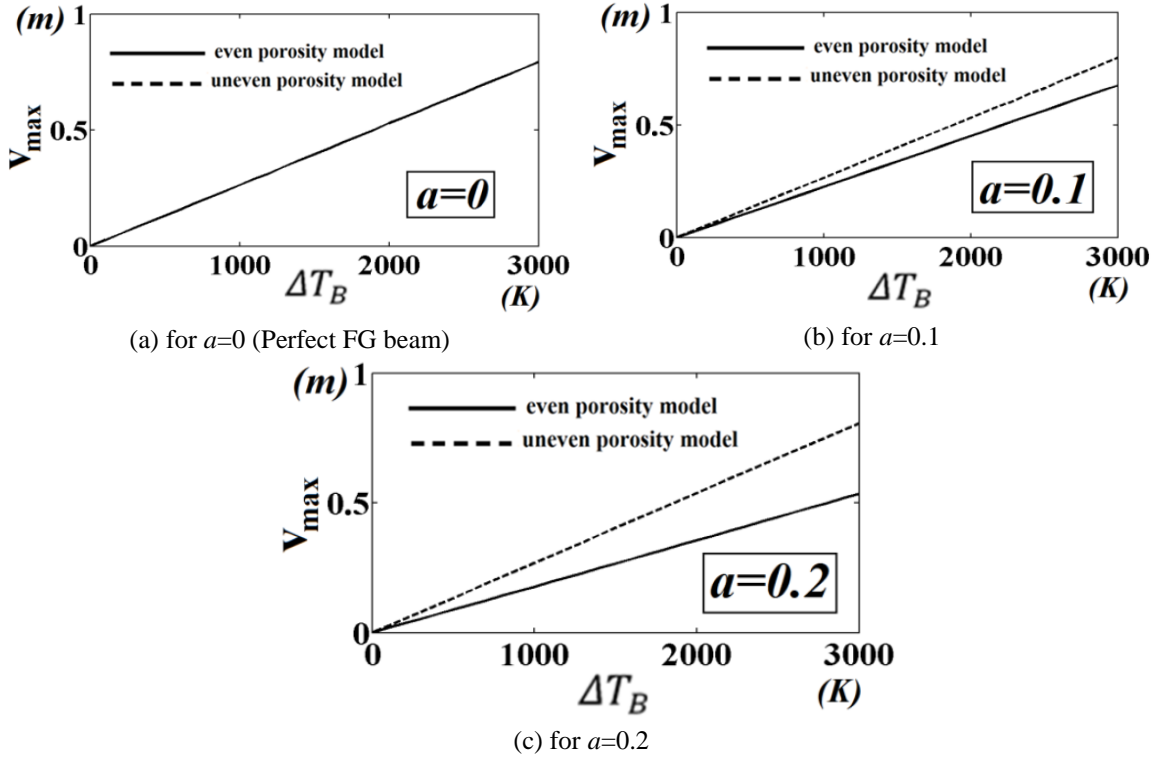
(b) for $a=0.1$

(c) for $a=0.2$

Fig. 6 Temperature rising-maximum vertical displacements (v_{max}) curves for different the porosity models in the temperature-independent physically property
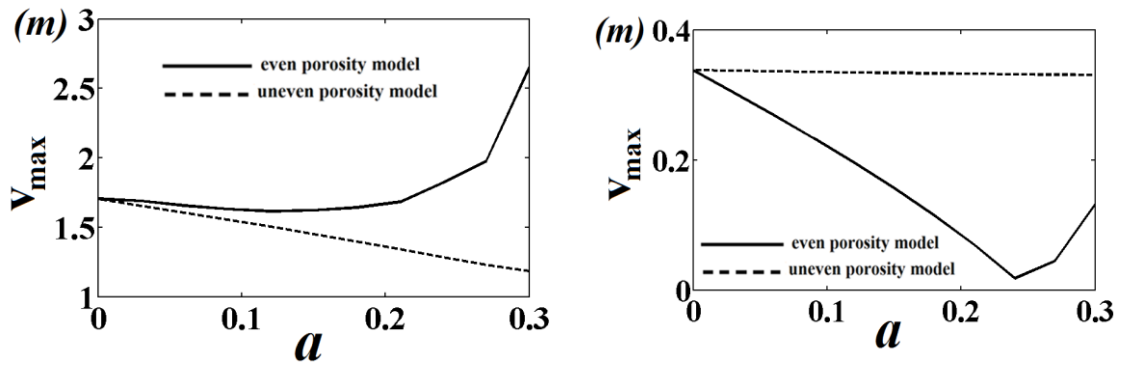

(a) for the temperature-dependent physically property

(b) for the temperature-independent physically property

Fig. 7 The effect of porosity parameter (a) and porosity models on the maximum large thermal displacements (v_{max}) of the FG porous beam

It is seen from Fig. 7 that increasing porosity parameter (a) up to a certain value, yields decreasing the deflections of the FG porous beams. After a certain value, the deflections increase significantly. It shows that the porosity is very effective in the thermal deflections after a certain value of the porosity parameter. Increase in the porosity parameter a, the difference between the
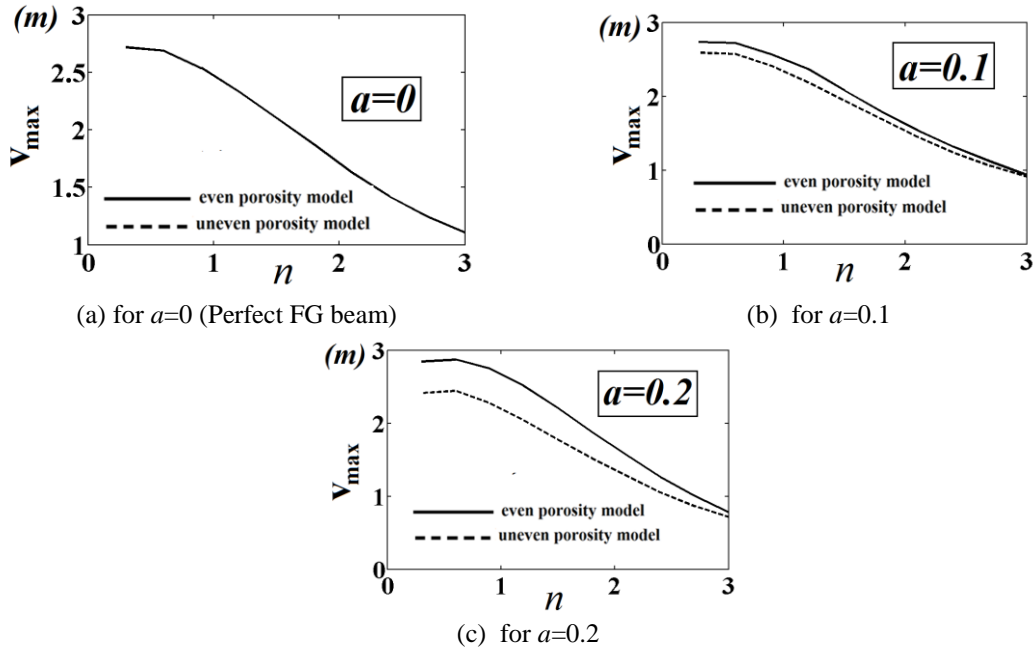
(a) for *a=0* (Perfect FG beam)

(b) for *a=0.1*

(c) for *a=0.2*

Fig. 8 The relationship between of the maximum vertical displacements (v_{max}) and the material distribution parameter *n* in the thermal deflections of the FG porous beam for different the porosity models in the temperature-dependent physically property

(a) for *a=0* (Perfect FG beam)
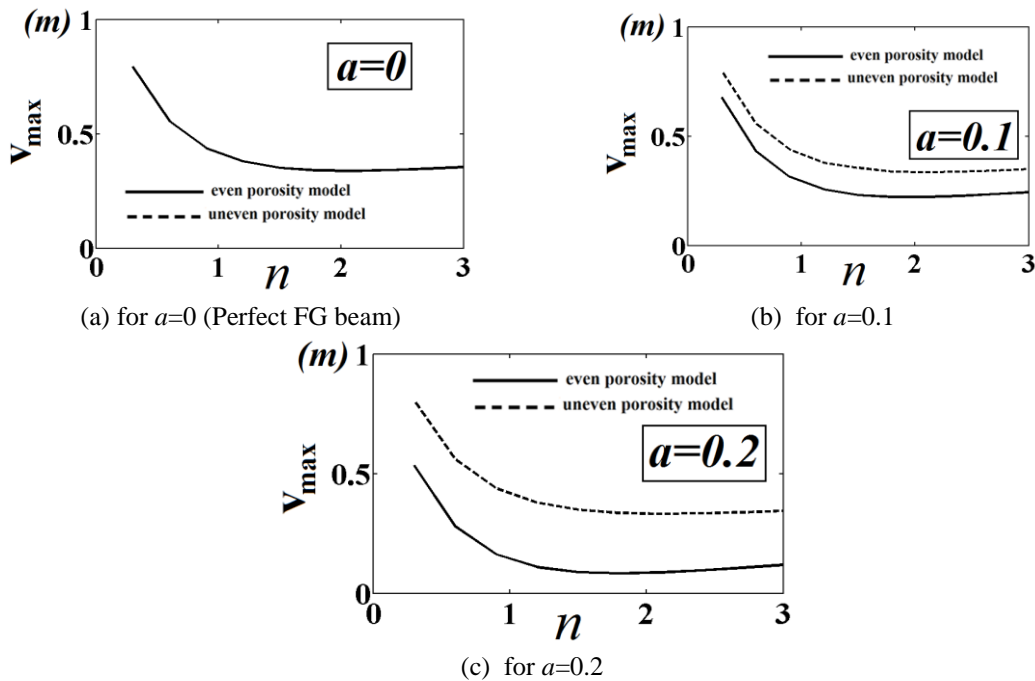
(b) for *a=0.1*

(c) for *a=0.2*

Fig. 9 The relationship between of the maximum vertical displacements (v_{max}) and the material distribution parameter *n* in the thermal deflections of the FG porous beam for different the porosity models in the temperature-independent physically property

even and uneven porosity models increases considerably as seen from Fig. 7. In higher values of porosity parameter *a*, the difference of porosity models is quite large. It shows that the porosity parameters have a very important role on the mechanical behavior of the FG porous beam. Similar to previous results, the results of the even porosity model are bigger than uneven model's in the temperature-dependent physically property as seen from Fig. 7. Whereas, the results of the uneven porosity model are bigger than even model's in the temperature-independent physically property.

In order to investigate the material distribution parameter *n* on the thermal nonlinear responses of the FG porous beam, the maximum transverse displacements obtained versus the material distribution parameter *n* for different porosity parameter and models in Figs. 8 and 9 for $\Delta T_B = 3000\,K$ and $\Delta T_T = 0$. The results of the Fig. 8 are obtained for the temperature-dependent physically property, whereas the results of the Fig. 9 are obtained for the temperature-independent physically property.

It is seen from Figs. 8 and 9 that the deflections of the beam increase with decrease in the power-law exponents *n*. With increase in the *n*, the beam gets to full Aluminum Oxide (bottom material) according to power-law function (Eqs. (1), (4) and (5)). The Young modulus of the Aluminum Oxide is smaller than Stainless Steel's (top material). This is as expected, due to the fact that an increase in the *n* can increase the elasticity modulus and bending rigidity of the beam decrease according to Eqs. (1) (4) and (3). As a result, the strength of the material increases. Another result of the Figs. 8 and 9, the difference between even and uneven porosity models decrease in the temperature-dependent physically property, however this difference increases in the temperature-independent physically property with increase *k* parameter. It shows that the material distribution plays an important role on the mechanical behaviour of the porous FG beam. It can be concluded from here: with the suitable choice of parameter, the negative effects of the porosity can be reduced. Also, it is seen from Figs. 8 and 9 that there is no difference between even and uneven porosity models in *a*=0, namely no porosity effect.

4. Conclusions

Nonlinear responses of functionally graded (FG) beams under thermal loading are investigated with porosity effect and the temperature dependent material properties. In the solution of the problem, total Lagrangian finite element is used in the 2-D solid continuum model within Newton-Raphson iteration method. The effects of material distribution, porosity parameters and temperature rising on the nonlinear deflections of the FG porous beam are studied and discussed for different porosity models. Also, the differences between temperature dependent and independent physical properties are investigated with porosity effects.

It is observed from the investigations; the main conclusions are as follows:

• Increase in the porosity parameter *a*, the difference between the even and uneven porosity models increases.

• Nonlinear deflection responses of FG beams significantly change in the temperature-dependent or independent physically properties.

• Increase in temperature, difference of the porosity models increase significantly.

• With decrease in the power-law exponent, the difference between even and uneven porosity models decrease in the temperature-dependent physically property.

• With decrease in the power-law exponent, the difference between even and uneven porosity models increase in the temperature-independent physically property.

• The nonlinear deflections in even porosity model are bigger than uneven model's in the temperature-dependent physically property.

• The nonlinear deflections in uneven porosity model are bigger than uneven model's in the temperature-independent physically property.

• The porosity and material distribution have very important role on the nonlinear behavior of the FG beam under temperature rising.

• With the suitable choice of material distribution parameter, the negative effects of the porosity can be reduced.

References

Agarwal, S., Chakraborty, A. and Gopalakrishnan, S. (2006), "Large deformation analysis for anisotropic and inhomogeneous beams using exact linear static solutions", *Compos. Struct.*, **72**(1), 91-104.

Akbarzadeh Khorshidi, M., Shariati, M. and Emam, S.A. (2016), "Postbuckling of functionally graded nanobeams based on modified couple stress theory under general beam theory", *J. Mech. Sci.*, **110**(1), 160-169.

Akbaş, Ş.D. and Kocatürk, T. (2011), "Post-buckling analysis of a simply supported beam under uniform thermal loading", *Sci. Res. Ess.*, **6**(5), 1135-1142.

Akbaş, Ş.D. (2013b), "Free vibration characteristics of edge cracked functionally graded beams by using finite element method", *J. Eng. Trends Technol.*, **4**(10), 4590-4597.

Akbaş, Ş.D. (2014), "Free vibration of axially functionally graded beams in thermal environment", *J. Eng. Appl. Sci.*, **6**(3), 37-51.

Akbaş, Ş.D. (2016a), "Post-buckling analysis of edge cracked columns under axial compression loads", *J. Appl. Mech.*, **8**(8), 1650086.

Akbaş, Ş.D. and Kocatürk, T. (2013), "Post-buckling analysis of functionally graded three- dimensional beams under the influence of temperature", *J. Therm. Stress.*, **36**(12), 1235-1254.

Akbaş, Ş.D. (2011), "Static analysis of a functionally graded beam with edge cracks on elastic foundation", *Proceedings of the 9th International Fracture Conference*, Istanbul, Turkey.

Akbaş, Ş.D. (2013), "Geometrically nonlinear static analysis of edge cracked timoshenko beams composed of functionally graded material", *Math. Prob. Eng.*, 14.

Akbaş, Ş.D. (2015a), "On post-buckling behavior of edge cracked functionally graded beams under axial loads", *J. Struct. Stab. Dyn.*, **15**(4)*,* 1450065.

Akbaş, Ş.D. (2015b), "Post-buckling analysis of axially functionally graded three dimensional beams", *J. Appl. Mech.*, **7**(3), 1550047.

Akbaş, Ş.D. (2015c), "Wave propagation of a functionally graded beam in thermal environments" *Steel Compos. Struct.*, **19**(6), 1421-1447.

Akbaş, Ş.D. (2016b) "Wave propagation in edge cracked functionally graded beams under impact force", *J. Vibr. Contr.*, **22**(10), 2443-2457.

Akbaş, Ş.D. (2017a), "Thermal effects on the vibration of functionally graded deep beams with porosity", *J. Appl. Mech.*, **9**(5), 1750076.

Akbaş, Ş.D. (2017b), "Post-buckling responses of functionally graded beams with porosities", *Steel Compos. Struct.*, **24**(5), 481-579-589.

Akbaş, Ş.D. (2017c), "Vibration and static analysis of functionally graded porous plates", *J. Appl. Comput. Mech.*, **3**(3), 199-207.

Akbaş, Ş.D. (2017d), "Stability of a non-homogenous porous plate by using generalized differantial quadrature method", *J. Eng. Appl. Sci.*, **9**(2), 147-155.

Akbaş, Ş.D. (2017e), "Free vibration of edge cracked functionally graded microscale beams based on the modified couple stress theory", *J. Struct. Stab. Dyn.*, **17**(3),1750033.

Akbaş, Ş.D. and Kocatürk, T. (2012), "Post-buckling analysis of Timoshenko beams with temperature-dependent physical properties under uniform thermal loading", *Struct. Eng. Mech.*, **44**(1), 109-125.

Al Jahwari, F. and Naguib, H.E. (2016), "Analysis and homogenization of functionally graded viscoelastic porous structures with a higher order plate theory and statistical based model of cellular distribution", *Appl. Math. Model.*, **40**(3), 2190-2205.

Almeida, C.A., Albino, J.C.R., Menezes, I.F.M. and Paulino, G.H. (2011), "Geometric   nonlinear analyses of functionally graded beams using a tailored Lagrangian formulation", *Mech. Res. Commun.*, **38**(8), 553-559.

Amara, K., Bouazza, M. and Fouad, B. (2016), "Postbuckling analysis of functionally graded beams using nonlinear model", *Period. Polytech. Eng. Mech. Eng.*, **60**(2), 121-128.

Anandrao, K.S., Gupta, R.K., Ramchandran, P. and Rao, V. (2010), "Thermal post-buckling analysis of uniform slender functionally graded material beams", *Struct. Eng. Mech.*, **36**(5), 545-560.

Babilio, E. (2014), "Dynamics of functionally graded beams on viscoelastic foundation", *J. Struct. Stab. Dyn.*, **14**(8), 1440014.

Ebrahimi, F. and Jafari, A. (2016), "A higher-order thermomechanical vibration analysis of temperature-dependent FGM beams with porosities", *J. Eng.*, 20.

Ebrahimi, F. Ghasemi, F. and Salari, E. (2016), "Investigating thermal effects on vibration behavior of temperature-dependent compositionally graded euler beams with porosities", *Meccan.*, **51**(1), 223-249.

Elmaguiri, M., Haterbouch, M., Bouayad, A. and Oussouaddi, O. (2015), "Geometrically nonlinear free vibration of functionally graded beams", *J. Mater. Environ. Sci.*, **6**(12), 3620-3633.

Fallah, A. and Aghdam, M.M. (2011), "Nonlinear free vibration and post-buckling analysis of functionally graded beams on nonlinear elastic foundation", *Eur. J. Mech. A/Sol.*, **30**(4), 571-583.

Hosseini, M. and Fazelzadeh, S.A. (2011), "Thermomechanical stability analysis of functionally graded thin-walled cantilever pipe with flowing fluid subjected to axial load", *J. Struct. Stab. Dyn.*, **11**(3), 513-534.

Hui-Shen, S. and Wang, Z.X. (2014), "Nonlinear analysis of shear deformable FGM beams resting on elastic foundations in thermal environments", *J. Mech. Sci.*, **81**, 195-206.

Jahwari, F. and Naguib, H.E. (2016), "Analysis and homogenization of functionally graded viscoelastic porous structures with a higher order plate theory and statistical based model of cellular distribution", *Appl. Math. Model.*, **40**(3), 2190-2205.

Kang, Y.A. and Li, X.F. (2009), "Bending of functionally graded cantilever beam with power-law non-linearity subjected to an end force", *J. Non-Lin. Mech.*, **44**(6), 696-703.

Kang, Y.A. and Li, X.F. (2010), "Large deflections of a non-linear cantilever functionally graded beam", *J. Reinf. Plast. Compos.*, **29**(12), 1761-1774.

Kar, V.R. and Panda, S.K. (2016), "Geometrical nonlinear free vibration analysis of FGM spherical panel under nonlinear thermal loading with TD and TID properties", *J. Therm. Stress.*, **39**(8), 942-959.

Ke, L.L., Yang, J. and Kitipornchai, S. (2009), "Postbuckling analysis of edge cracked functionally graded Timoshenko beams under end shortening", *Compos. Struct.*, **90**(2), 152-160.

Kocatürk, T., Şimşek, M. and Akbaş, Ş.D. (2011), "Large displacement static analysis of a cantilever Timoshenko beam composed of functionally graded material", *Sci. Eng. Compos. Mater.*, **18**, 21-34.

Kocatürk, T. and Akbaş, Ş.D. (2010), "Geometrically non-linear static analysis of a simply supported beam made of hyperelastic material", *Struct. Eng. Mech.*, **35**(6), 677-697.

Kocatürk, T. and Akbas, Ş.D. (2011), "Post-buckling analysis of Timoshenko beams with various boundary conditions under non-uniform thermal loading", *Struct. Eng. Mech.*, **40**(3), 347-371.

Kocatürk, T. and Akbaş, Ş.D. (2012), "Post-buckling analysis of Timoshenko beams made of functionally graded material under thermal loading", *Struct. Eng. Mech.*, **41**(6), 775-789.

Kocatürk, T. and Akbaş, Ş.D. (2013), "Thermal post-buckling analysis of functionally graded beams with temperature-dependent physical properties", *Steel and Composıte Structures*, **15**(5), 481-505-1254.

Kolakowski, Z. and Teter, A. (2015), "Static interactive buckling of functionally graded columns with closed cross-sections subjected to axial compression", *Compos. Struct.*, **123**(1), 257-262.

Li, L.Q. and Shao, Q.H. (2014), "Non-linear analysis of a FGM cantilever beam supported on a winkler elastic foundation", *Appl. Mech. Mater.*, **602**, 131-134.

Li, Q. and Li, S. (2011), "Post-bucking configuration of a functionally graded material column under distributed load", *Fuhe Cailiao Xuebao(Acta Mater. Compos. Sin.)*, **28**(3), 192-196.

Li, S.R., Zhang, J.H. and Zhao, Y.G. (2006), "Thermal post-buckling of functionally graded material timoshenko beams", *Appl. Math. Mech.*, **26**(6), 803-810.

Mechab, B., Mechab, I., Benaissa, S., Ameri, M. and Serier, B. (2016b), "Probabilistic analysis of effect of the porosities in functionally graded material nanoplate resting on Winkler-Pasternak elastic foundations", *Appl. Math. Modell.*, **40**(2),738-749.

Mechab, I., Mechab, B., Benaissa, S., Serier, B. and Bouiadjra, B.B. (2016a), "Free vibration analysis of FGM nanoplate with porosities resting on Winkler Pasternak elastic foundations based on two-variable refined plate theories", *J. Brazil. Soc. Mech. Sci. Eng.*, **38**, 2193-2211.

Mohanty, S.C., Dash, R.R. and Rout, T. (2012), "Static and dynamic stability analysis of a functionally graded timoshenko beam", *J. Struct. Stab. Dyn.*, **12**(4), 33.

Nguyen, D.K., Gan, B.S. and Trinh, T.H. (2014), "Geometrically nonlinear analysis of planar beam and frame structures made of functionally graded material", *Struct. Eng. Mech.*, **49**(6), 727-743.

Rastgo, A., Shafie, H. and Allahverdizadeh, A. (2005), "Instability of curved beams made of functionally graded material under thermal loading", *J. Mech. Mater. Des.*, **2**, 117-128.

Reddy, J.N. and Chin, C.D. (1998), "Thermoelastical analysis of functionally graded cylinders and plates", *J. Therm. Stress.*, **21**(6) 593-626.

Reddy, J.N. (2004), *An Introduction to Non-Linear Finite Element analysis*, Oxford University Press Inc, New York, U.S.A.

Şimşek, M. and Aydın, M. (2017), "Size-dependent forced vibration of an imperfect functionally graded (FG) microplate with porosities subjected to a moving load using the modified couple stress theory", *Compos. Struct.*, **160**, 408-421.

Song, X. and Li, S. (2008), "Nonlinear stability of fixed-fixed FGM arches subjected to mechanical and thermal loads", *Adv. Mater. Res.*, **33-37**, 699-706.

Sun, Y., Li, S.R. and Batra, R.C. (2016), "Thermal buckling and post-buckling of FGM timoshenko beams on nonlinear elastic foundation", *J. Therm. Stress.*, **39**(1) 11-26.

Touloukian, Y.S. (1967), *Thermophysical Properties of High Temperature Solid Materials*, Macmillan, New York, U.S.A.

Trinh, T.H., Nguyen, D.K., Gan, B.S. and Alexandrov, S. (2016), "Post-buckling responses of elastoplastic FGM beams on nonlinear elastic foundation", *Struct. Eng. Mech.*, **58**(3), 515-532.

Wattanasakulpong, N. and Ungbhakorn, V. (2014), "Linear and nonlinear vibration analysis of elastically restrained ends FGM beams with porosities", *Aerosp. Sci. Technol.*, **32**(1), 111-120.

Yan, T., Yang, J. and Kitipornchai, S. (2012), "Nonlinear dynamic response of an edge-cracked functionally graded timoshenko beam under parametric excitation", *Nonlin. Dyn.*, **67**(1), 527-540.

Zhang, D.G. and Zhou, H.M. (2014), "Nonlinear bending and thermal post-buckling analysis of FGM beams resting on nonlinear elastic foundations", *CMES Comput. Modell. Eng.*, **100**(3) 201-222.

CC